Journal of Alloys and Compounds 517 (2012) 103–110

Contents lists available at SciVerse ScienceDirect

Journal of Alloys and Compounds

journal homepage: www.elsevier.com/locate/jallcom

Spectroscopic studies on Fe^{3+} doped CdS nanopowders prepared by simple coprecipitation method

H. Sekhar, D. Narayana Rao*

University of Hyderabad, Hyderabad – 500 046, India

ARTICLE INFO

Article history:
Received 6 September 2011
Received in revised form 9 December 2011
Accepted 12 December 2011
Available online 19 December 2011

Keywords:
Nanopowders
Luminescence
Electron spin resonance
Raman scattering

ABSTRACT

Nanopowders of PVP capped undoped, and Fe doped cadmium sulfide (CdS:Fe) were prepared by a simple co-precipitation method at room temperature, mixing the stoichiometric amount of reactants in a Milli Q water solvent. Spectral characteristics of as prepared nanopowders were investigated by using XRD, FTIR, Raman, UV-Vis absorption, FE-SEM-EDAX, Photoluminescence and ESR at room temperature. Extremely broad reflections of XRD peaks of as prepared powders are in nanometer size and cubic structure. Doping with Fe in CdS does not lead to any structural phase transformation but introduces a slight decrease in the lattice constants. Raman spectrum of pure and Fe doped CdS nanopowders has two characteristic LO phonon peaks. Raman spectrum of Fe doped CdS nanopowders shifts slightly towards higher energy side compared to their pure CdS nanopowders. Electron phonon confinement factor (S) varies in between 0.2 and 0.4. Photoluminescence emission spectrum shows a peak at 404 nm which is attributed to localized band edge emission. At lower doping of Fe (5%, 10%) the emission intensity increases and for higher doping (20%) the emission intensity gets quenched. The electron spin resonance spectra of Fe doped CdS exhibit two distinct signals at $g \sim 4.3$ and $g \sim 2$ characteristic of Fe^{3+} ions.

1. Introduction

Semiconductor nanoparticles or quantum dots (QDs) with typical dimensions of 1–100 nm have generated enormous attention in the past decades because their optical and electronic properties are dramatically different from those of the corresponding bulk crystals and also because of their wide applications in the fields of optoelectronic and biological technology [1–7]. Chalcogenide semiconductors such as cadmium sulfide is a well characterized II–VI group inorganic semiconductor with a wide direct band gap of 2.42 eV (bulk CdS) and a small exciton Bohr radius of 2.5 nm. The nanoparticle radius is comparable to the Bohr exciton radius in the corresponding bulk material, leading to splitting of continuum of electronic energy levels into discrete states with the effective band gap energy blue shifted from that of the bulk. II–VI semiconductor nanostructures have been investigated widely and demonstrated potential application in solar cells [1], light emitting diodes [2], IR photodetectors [3], electrically driven lasers [4], optical limiters [5] biological fluorescent labels [6] and upconversion luminescent materials [7]. Semiconductor nanocrystals have been prepared either as powder or stable self standing nanocrystals by using different organic stabilizers to prevent them from aggregation by capping their surfaces.

Doping with different metal ions or crystal imperfections (sulfur and cadmium vacancies) can act as donors and acceptor in CdS [8]. Fe based II–VI semiconductor materials such as $Cd_{1-x}Fe_xTe$, $Cd_{1-x}Fe_xSe$, $Zn_{1-x}Fe_xTe$, $Zn_{1-x}Fe_xS$ and $Cd_{1-x}Fe_xS$ have been studied by many workers [9–15]. However reports on preparation, optical [14,15] and electron spin resonance (ESR) properties of Fe-doped CdS nanopowders are few.

The optical and magnetic properties of transition metal ions doped II–VI nanomaterials differ from the corresponding host nanomaterials. These impurities can strongly modify the luminescence properties because they provide impurity centers that interact with the quantum confined electron hole pair. The crystallite luminescence is a strong function of the surface characteristics. Usually, two type's emissions are observed from semiconductor nanoparticles: an excitonic and a trap (defect) emission. When CdS is prepared in stoichiometric quantities of Cd and S, it will emit blue light emission. Formation of CdS particles in the environment of excess amount of Cd^{2+} or S^{2-} will results in several trap states. CdS containing excess S^{2-} generates orange or red light emission while excess of Cd^{2+} leads to yellow emission [16–18]. It is well known that iron acts as fluorescence quencher in II–VI semiconductors [12,13]. Since these impurities can be paramagnetic, they introduce a localized spin into the nanocrystal, and form the so called diluted magnetic semiconductors (DMS). DMSs are II–VI,

* Corresponding author. Tel.: +91 40 23134335; fax: +91 40 23010227.
E-mail addresses: dnrsp@uohyd.ernet.in, dnr.laserlab@gmail.com (D.N. Rao).

0925-8388/$ – see front matter © 2011 Elsevier B.V. All rights reserved.
doi:10.1016/j.jallcom.2011.12.039

IV–VI, or III–V compounds in which fraction of nonmagnetic cations have been substituted by magnetic transition metal or rare-earth metal ions [19]. Room-temperature ferromagnetism observed in transition metal [10] and rare earth doped semiconductors has triggered the current intense interest in spintronic materials. Apart from room temperature ferromagnetism of the nanoparticles, it is also important to tune the magnetic properties of the nanoparticles. Although size tuning is one option, doping of the nanoparticles is another possibility. Thrust of recent research has been on the synthesis and study of the physical properties of nano scale doped CdS nanoparticles such as solid powder by simple techniques.

This paper focuses on the synthesis of stoichiometric amount of Fe-doped CdS nanopowders with cubic structure, the effect of iron (Fe) doping concentration and on its physical properties at room temperature. The method used is rather simple and inexpensive, in which reaction is carried out at room temperature. Raman and IR spectroscopy was employed to investigate vibrational states of as prepared powders. Electron Spin Resonance (ESR) studies were carried out on Fe doped CdS nanopowders in order to determine the oxidation state of dopant ions in the host lattice.

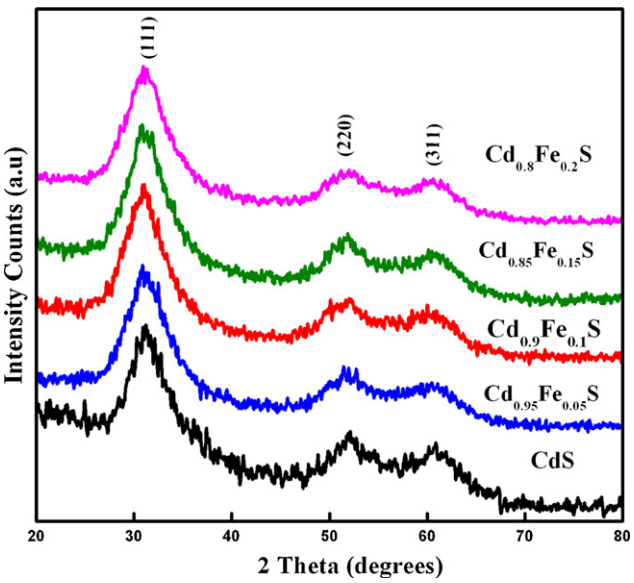

Fig. 1. The XRD pattern of pure and Fe doped CdS nanopowders.

2. Experimental

2.1. Preparation technique

Nanopowders of PVP capped pure and Fe doped CdS nanoparticles were prepared by the colloidal chemical precipitation method using cadmium acetate dihydrate ($Cd(CH_3COOH)_2{\cdot}2H_2O$), iron nitrate nonahydrate ($Fe(NO_3)_3{\cdot}9H_2O$), and sodium sulfide (Na_2S) as the starting compounds at room temperature in air. In a typical synthesis, first 30 ml of 0.1 M Na_2S solution and solutions with different molar ratios of cadmium acetate to iron (III) nitrate of 10:0, 9.5:0.5, 9:1, 8.5:1.5, and 8:2 were prepared. At room temperature about 15 ml of polyvinyl pyrrolidone (PVP MW-55,000) solution in methanol (0.5 M) was added to 30 ml of the solution of Cd–Fe mixed solution with vigorous stirring. 0.1 M Na_2S solution was added slowly drop wise to the Cd, Fe mixed solution under vigorous stirring. After 90 min stirring the precipitated particles were isolated from the solution by centrifuging at 6000 rpm for 15 min. The product was washed by Milli Q water and methanol through multiple cycles of centrifuging and redispersion. The yellow, orange precipitate obtained was washed and air dried. Prepared powders were analyzed through different techniques.

2.2. Instruments

X-ray diffractograms (XRD) on the dried precipitate were recorded using powder X-ray diffractometer (Inel C120) which is equipped with a curved position sensitive detector and data was collected using Co-Kα radiation of wavelength 0.17889 nm. The grain size of the as prepared powders was calculated according to the X-ray line-broadening method using the Scherrer's equation, $d = 0.99\lambda/\beta \cos\theta$, where d is the average crystalline grain size; λ is the X-ray wavelength; β is the FWHM of diffraction peak; and θ corresponds to the peak position. The information on the structure and bond formation of CdS powders were analyzed from the IR spectroscopy with KBr powder from Sigma–Aldrich as reference material. The IR spectra were measured from 400 to 4000 cm^{-1} on JASCO FT/IR-5300 spectrometer operating at a resolution of 4 cm^{-1}. Raman spectra, which gives detailed information on the vibrational spectra, was obtained using Horiba Jobin Yvon LabRam HR high resolution micro-Raman spectrograph with 514.5 nm of Argon ion laser as the excitation source. The Raman instrument was calibrated with a standard Si wafer (wavenumber 520 cm^{-1}) before and after recording. The laser light was focused on the powder sample with a 20X objective lens and the back-scattered light was collected into the LabRam spectrometer equipped with grating having 1800 groves/mm. FE-SEM-EDAX analysis was carried out on a Carl Zeiss Ultra 55 model. UV–Visible spectral analysis was carried out on a JASCO UV-Visible absorption spectrophotometer with a resolution of 1 nm between 200 and 800 nm with a scanning speed of 200 nm/min. Steady-state photoluminescence (PL) characteristics of as prepared powders dispersed in chloroform placed in a 1 cm path non-fluorescent quartz cuvette, were measured by Jobin Yvon Inc., Fluorolog 3 spectrofluorometer with a spectral resolution of 1 nm, excitation wavelengths were typically around 280–360 nm. The ESR spectrum was obtained with the as-synthesized powders kept in a 4 mm diameter quartz tube. For this all the samples of equal weight were taken and measurements were done at room temperature. Spectra were recorded as a first derivative with modulation frequency 100 kHz. The settings used in recording the ESR spectra were as follows: modulation amplitude is 10 G, frequency is 9.15138 GHz, and power is 0.9980 mW.

3. Results and discussions

3.1. XRD

X-ray diffraction (XRD) studies of the pure and Fe doped CdS powders reflection peaks were broadened and as shown in Fig. 1. It can be attributed to a very small grain size of the particles. The reflection peaks of as synthesized powders can be indexed to be cubic phase, has three main peaks at 30.92°, 51.6° and 61.39° (referring to (1 1 1), (2 2 0) and (3 1 1) planes) with JCPDS data card no. 800019 at Co-Kα radiation of wavelength 0.17889 nm. Since we did not observe any characteristic peaks of the impurity phases in the XRD spectrum, we have concluded that the dopant is distributed homogenously without clustering or segregation [20]. Using XRDA software we calculated lattice parameters of pure and doped CdS powders. Table 1 shows the lattice parameters of pure and Fe doped CdS and its crystallite size calculated from the full width at half maximum (FWHM) of the diffraction peaks using the Debye–Scherrer formula. The ionic radius of Fe^{3+} (0.64 Å) ion is smaller than that of Cd^{2+} (0.97 Å) ion. Therefore doping with Fe in CdS may not lead to any structural phase transformation but introduces a decrease in the lattice constants.

Table 1
Lattice parameter and its crystallite size for pure and Fe doped CdS nanopowders.

Sample	Lattice parmeter '*a*' (Å)	Crystallite size (Scherrer formula) (nm)
CdS	5.7941	3.9
$Cd_{0.95}Fe_{0.05}S$	5.7802	3.7
$Cd_{0.9}Fe_{0.1}S$	5.7730	3.4
$Cd_{0.85}Fe_{0.15}S$	5.7342	3.2
$Cd_{0.8}Fe_{0.2}S$	5.7098	2.8

3.2. FTIR studies

Fourier transform infrared spectroscopy (FTIR) spectra have long been used to identify organic and inorganic materials by measuring the absorption of various infrared light wavelengths. The FTIR spectrum of pure and Fe doped CdS powders is as shown in Fig. 2. In the higher energy region the peak at 3420 cm^{-1} is assigned to O—H stretching, peak at 1635 cm^{-1} is assigned to bending (H—O—H) vibration of the water absorbed on the surface of CdS [21]. The peak at 1417 cm^{-1} is assigned to bending vibration of methanol used in the process. The C—O stretching vibration of absorbed methanol gives peak at 1098 cm^{-1}. The absorption band at 620 cm^{-1} has been assigned to Cd—S stretching.

3.3. Raman studies

Raman scattering is a nondestructive and inelastic process to obtain information on the vibrational states of a solid. In the last few years, the studies of quantum size effects were mainly focused on the observation of the shift of Raman peaks [22,23]. LO phonon peaks of bulk CdS has two characteristics of 1-LO (first harmonic (at 300 cm^{-1})) and 2-LO (second harmonic (at 600 cm^{-1})) vibrations [24]. The sharp characteristics of the two LO phonon peaks in pure and Fe doped CdS, as shown in Fig. 3, are indicative of the good surface condition of the nanopowders. Intensity of the 1-LO is stronger than that of the 2-LO for all samples. Variation in the observed energies for pure CdS nanoparticles at 293, 593 cm^{-1} in comparison to their bulk values might be the result of quantum confinement. Similar results were reported in earlier studies on CdS nanowires [22], where a 7 cm^{-1} decrease was observed when the particle size varied from 22 to 9 nm. In the Fe doped CdS samples the 1-LO and 2-LO modes shift towards higher energy side compared to their pure CdS nanopowders. Similar results were also observed in the

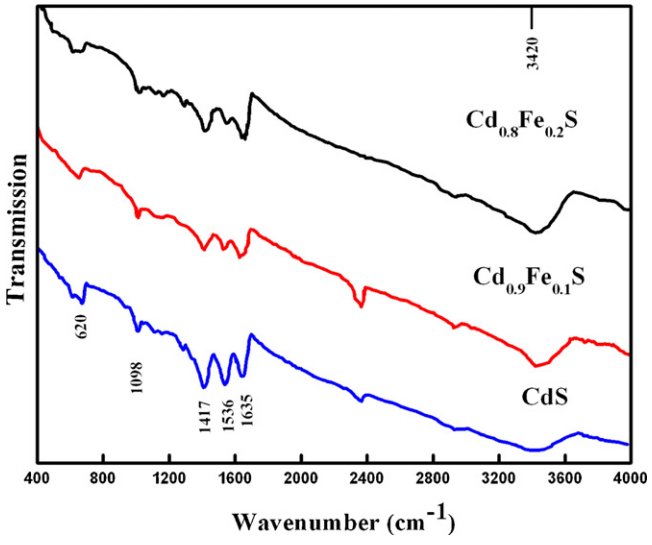

Fig. 2. FTIR spectrum of pure and Fe doped CdS nanopowders.

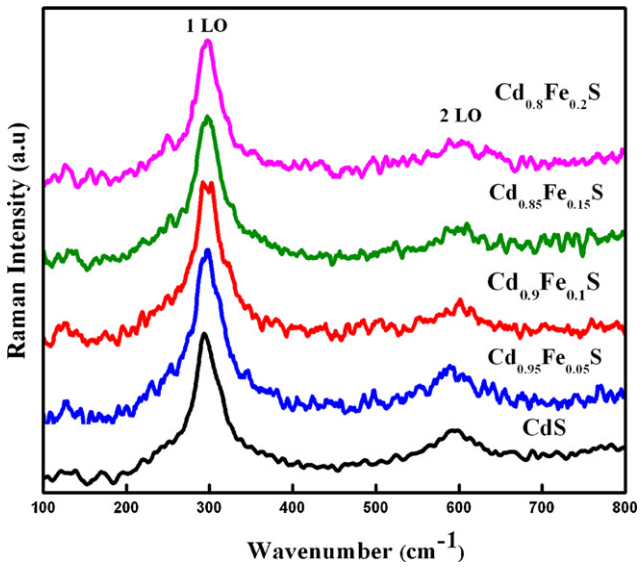

Fig. 3. Raman spectrum of pure and Fe doped CdS nanopowders.

case Zn doped CdS nanocrystals prepared by different methods [25]. Increasing Fe concentration in $Cd_{1-x}Fe_xS$ nanopowders, the Raman intensities of two LO modes become weaker, which may be related to their poorer crystallinity, increased compositional and structural disorders [25]. The ratio of 2-LO mode intensity to 1-LO mode intensity (I_{2LO}/I_{1LO}) is a parameter used to specify exciton–phonon coupling strength (S) in the semiconductors [24]. Table 2 shows the calculated exciton–phonon coupling strength and 1-LO mode full width half maximum (FWHM) for as prepared powders. Our observations are in agreement with an earlier reported decrease in ratio (S) from 0.88 to 0.42 from bulk to nanospheres at 514.5 nm excitation [24]. The phenomenon may be attributed to lowering of the exciton–vibration coupling due to quantum confinement.

3.4. FE-SEM-EDAX studies

The overall morphology, elemental quantification and stoichiometric ratio of freshly prepared pure and Fe doped CdS powders mounted on double sided carbon tape, were inferred from FE-SEM-EDAX studies. Field emission scanning electron microscope (FE-SEM) images of as synthesized powders are shown in Fig. 4. The FE-SEM image with different magnifications clearly indicates the formation of nanoclusters. The grains have aggregated to form clusters. Fig. 5 shows EDAX analysis of the as synthesized powders. From the clear peaks of cadmium (Cd), iron (Fe) and sulfur (S) it is noted that our sample did not show any traces of other elements. The compositional ratio, as calculated from chemical formula and EDAX analysis, are compared in Table 3. It confirms that the Cd/Fe in the nanocrystals is approximately same as that of the reactants ratio over a large composition range. A repeat of the experiment at

Table 2
Raman shift and exciton phonon confinement factor for pure and Fe doped CdS.

Sample	Raman shift (cm^{-1})		Exciton phonon confinement factor (S)	FWHM (cm^{-1})
	1-LO	2-LO		
CdS	293	593	0.3913	37.12
$Cd_{0.95}Fe_{0.05}S$	298	598	0.2937	41.40
$Cd_{0.9}Fe_{0.1}S$	297	599	0.2039	39.97
$Cd_{0.85}Fe_{0.15}S$	297	600	0.2126	38.21
$Cd_{0.8}Fe_{0.2}S$	298	600	0.2325	32.72

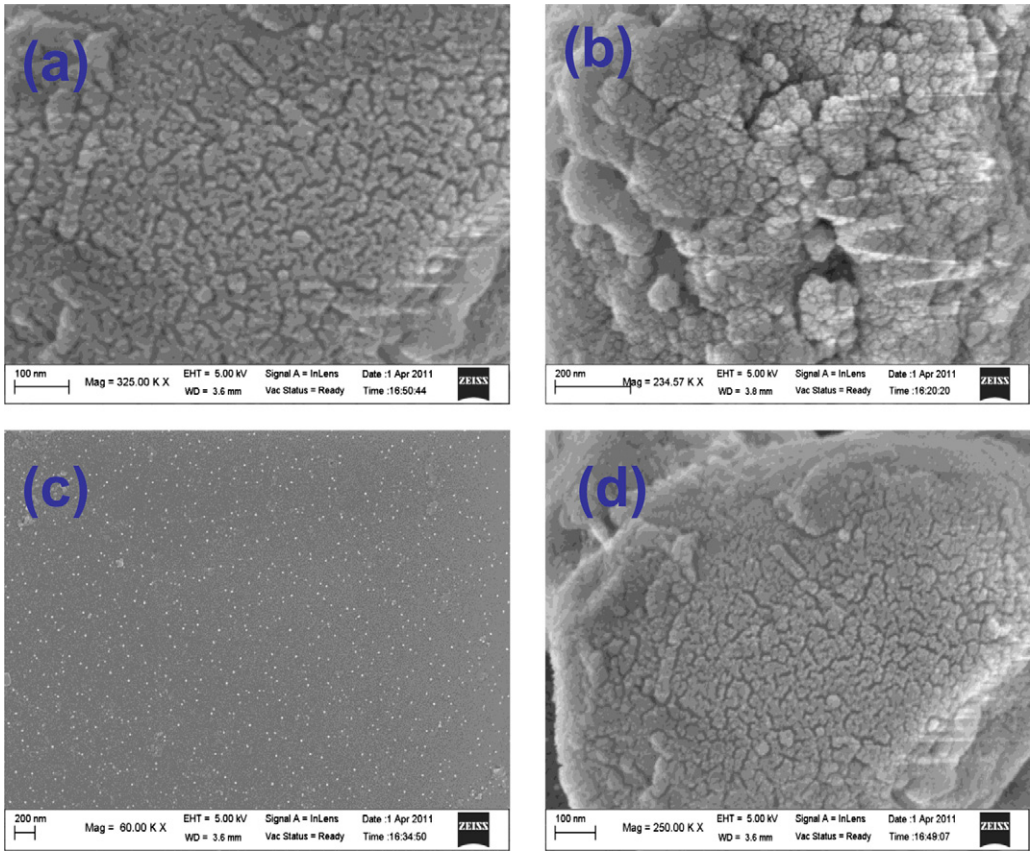

Fig. 4. FE-SEM images of (a) CdS, (b) $Cd_{0.95}Fe_{0.05}S$, (c) $Cd_{0.85}Fe_{0.15}S$ and (d) $Cd_{0.8}Fe_{0.2}S$ powders.

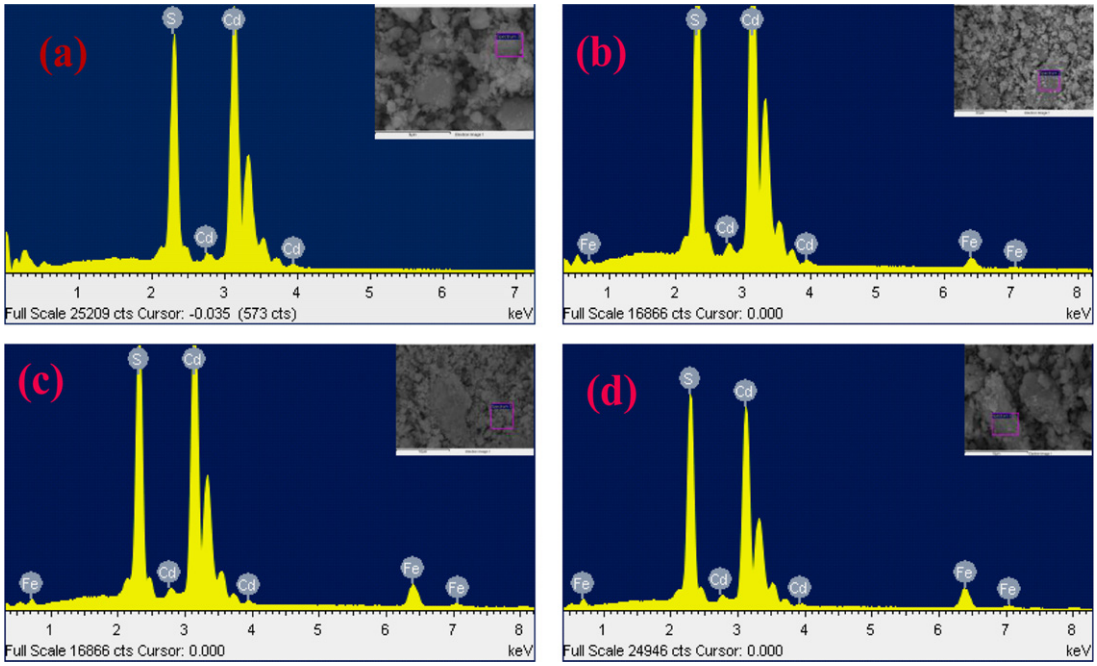

Fig. 5. EDAX spectrum of (a) CdS, (b) $Cd_{0.95}Fe_{0.05}S$, (c) $Cd_{0.85}Fe_{0.15}S$ and (d) $Cd_{0.8}Fe_{0.2}S$.

Table 3
The compositional ratio of pure and Fe doped CdS, calculated from chemical formula and EDAX analysis.

Sample	Elements (at.%)					
	From chemical formula			From EDAX analysis		
	Cd	S	Zn	Cd	S	Zn
CdS	50	50	0	50.09	49.01	0
$Cd_{0.95}Fe_{0.05}S$	47.5	50	2.5	46.82	50.53	2.65
$Cd_{0.9}Fe_{0.1}S$	45	50	5	44.93	51.02	4.05
$Cd_{0.85}Fe_{0.15}S$	42.5	50	7.5	42.57	51.13	6.30
$Cd_{0.8}Fe_{0.2}S$	40	50	10	40.90	50.51	8.59

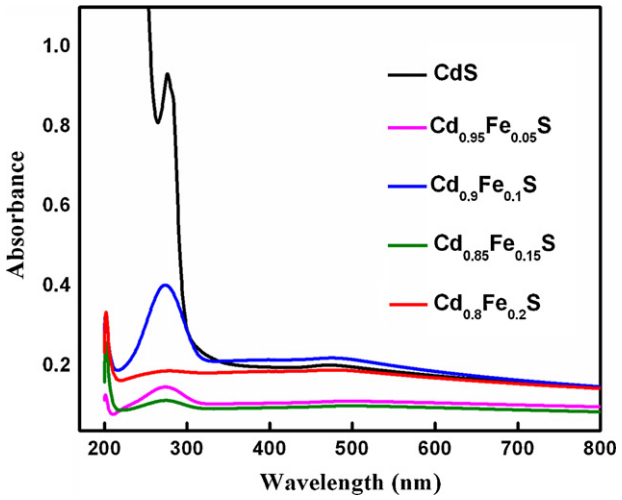

Fig. 6. UV–Vis absorption spectrum of pure and Fe doped CdS nanopowders.

different locations yielded the same result. This confirms the successful doping of Fe in place of Cd in our method of preparation of the CdS nanopowders.

3.5. UV–Vis absorption spectroscopy

UV–Visible absorption spectroscopy is an efficient technique to monitor the optical properties of quantum-size particles. Absorption spectrum was recorded for pure and Fe doped CdS nanopowders dispersed in chloroform and ultrasonicated for 15 min. Fig. 6 shows that the absorption spectrum of pure and Fe doped CdS powders are blue-shifted relative to bulk CdS (~2.42 eV

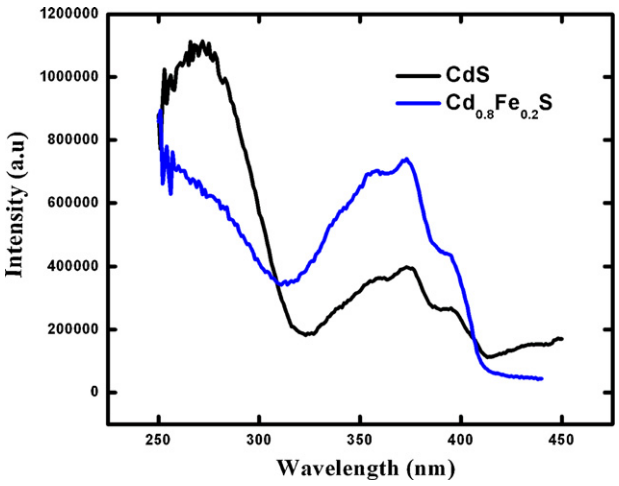

Fig. 7. Excitation spectrum of CdS and $Cd_{0.8}Fe_{0.2}S$ nanoparticles in chloroform.

(512 nm)) due to quantum confinement effects, suggesting the formation of nanometer-sized CdS particles. The broad absorption peak around 460–480 nm is attributed as due to the surface states of the aggregated particles [24] and the narrow peak around 280 nm is attributed as due to the exciton peak of CdS. Absorption peak at 280 nm shows broadening in the case of Fe doped CdS compared to their pure CdS, which could mean that the exciton peak energies in the doped system are distributed over wide energies. Henglein and co-workers [26] have shown that the absorption at 500 nm corresponds to a particle diameter of ~6 nm. Based on these results, we believe that as-synthesized pure and Fe doped CdS powders are less than 6 nm.

3.6. Photoluminescence (PL) studies

As prepared solid nanopowders (4×10^{-4} M) were dispersed in chloroform through 15 min ultrasonication. The spectra were recorded, keeping the spectrometer settings (slit widths and scanning rates) the same for all the recordings. We have monitored the effect of iron doping on the photoluminescence intensity. An excitation spectrum was recorded monitoring 454 nm and as shown in Fig. 7. We show the variation in the emission spectra due to excitation in to the excitonic band and the defect band.

At different excitations pure and Fe (20%) doped CdS emission spectrum are shown in Figs. 8 and 9. At lower wavelength excitation pure and Fe (5%, 10%, 15%) doped CdS shows a broad

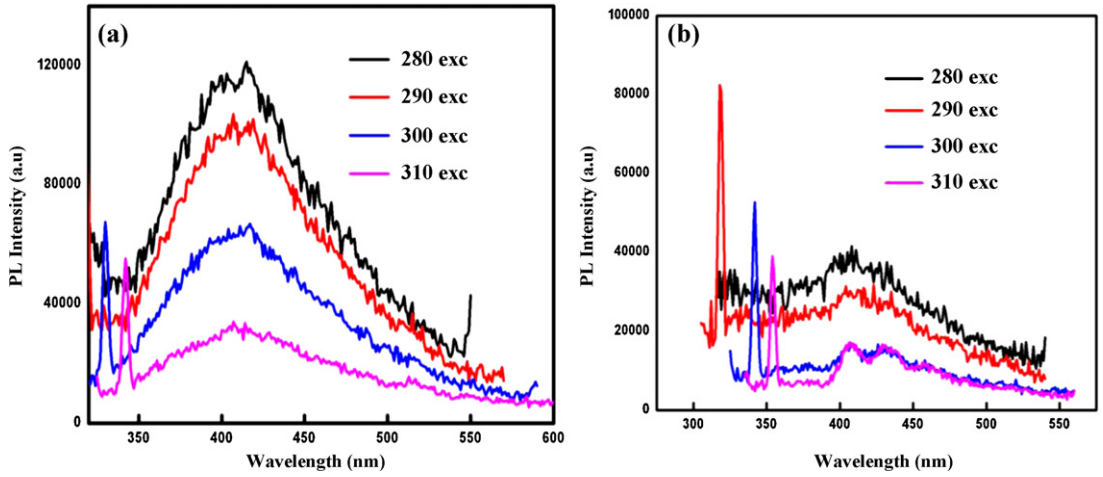

Fig. 8. Photoluminescence spectrum of (a) CdS and (b) $Cd_{0.8}Fe_{0.2}S$ powders (lower wavelength excitation).

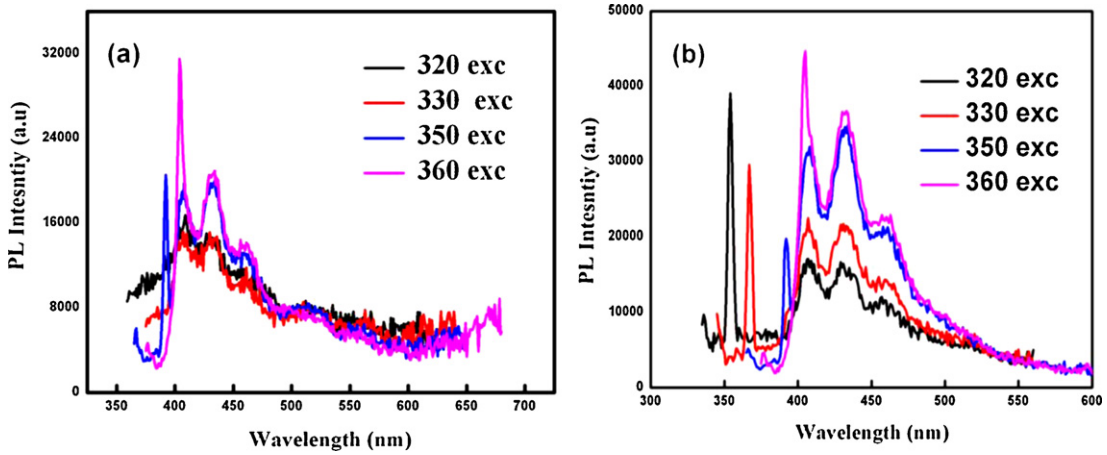

Fig. 9. Photoluminescence spectrum of (a) CdS and (b) $Cd_{0.8}Fe_{0.2}S$ powders (longer wavelength excitation).

emission centered at 404 nm is observed. Fig. 10 shows the comparison of photoluminescence intensity of pure and Fe doped CdS at 290 nm excitation. At low dopings (Fe 5%, 10%) the emission intensity increases. At 15% dopings the emission intensity approximately equal to their pure CdS as shown in Fig. 10. Further increasing doping to $x = 0.2$ the emission intensity decreases rapidly. It was reported that this kind of band-edge luminescence is caused by the recombination of shallow region trapped electron–hole pairs and/or excitons [27,28]. The absence of emission from trap (defect) states suggests the stoichiometric nature of CdS, without a surface excess of Cd^{2+} or S^{2-} vacancies. The attenuation of the fluorescence is attributed to self quenching, means iron act as electron trapping centers which results into nonradiative recombination [12]. This means that photo-excited electrons are preferentially transferred to iron metal ion induced trapping centers.

With longer wavelength excitations (320–360 nm), broad emission peak splits in to multiple peaks as shown in Fig. 9 (long wavelength excitations). It is quite interesting to see that as one moves towards the longer wavelength excitation, the emission starts showing well resolved emission peaks in the spectrum. This is attributed to the select band edge sites that get excited leading to the emission from these excited states without getting diffused in to the other sites. This localized emission could play an important role in the site selection spectroscopy. The broad emission from the CdS bandgap (for excitations less than 310 nm) is also quite distinguishable from the spectra due to the band edge states (for excitations longer than 310 nm), which exhibits well resolves peaks.

The narrow feature that appears at about 306 nm with 280 nm excitation is identified as one due to the CH Raman stretching band ($3018\ cm^{-1}$) of the solvent (chloroform). The position of this feature shifts with the excitation wavelength. With higher energy excitations CdS luminescence becomes much stronger while the Raman band becomes comparatively negligible.

3.7. ESR spectral studies

To probe the exact oxidation state of the dopant ion we have carried out ESR spectral studies at room temperature on Fe doped CdS nanopowders as shown in Fig. 11. No resonance signal is observed from pure CdS. The effective g-factor is determined according to the equation

$$g = \frac{h\gamma}{\mu_B H}$$

where h is Planck's constant, γ is the microwave frequency and μ_B is the Bohr magneton. For increasing the doping concentration the integrated intensity could increase, that confirms that Fe^{3+}

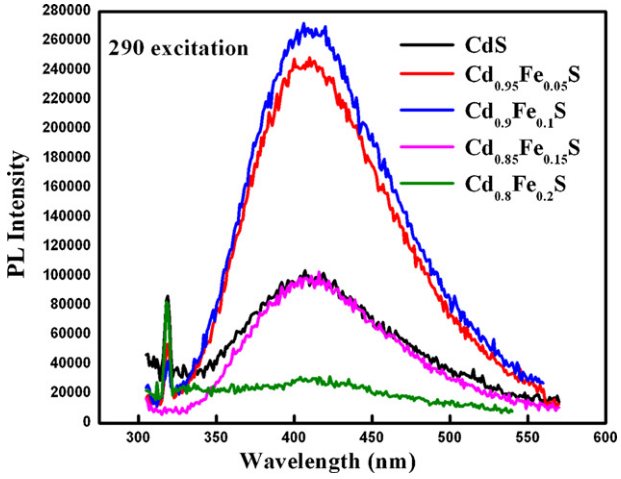

Fig. 10. Comparison of photoluminescence of pure and Fe doped CdS at 290 nm excitation.

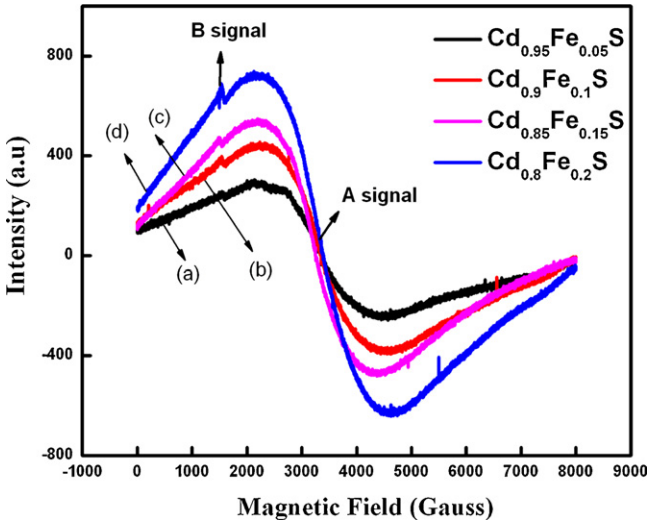

Fig. 11. ESR spectrum of (a) $Cd_{0.95}Fe_{0.05}S$, (b) $Cd_{0.9}Fe_{0.1}S$, (c) $Cd_{0.85}Fe_{0.15}S$ and (d) $Cd_{0.8}Fe_{0.2}S$ powders.

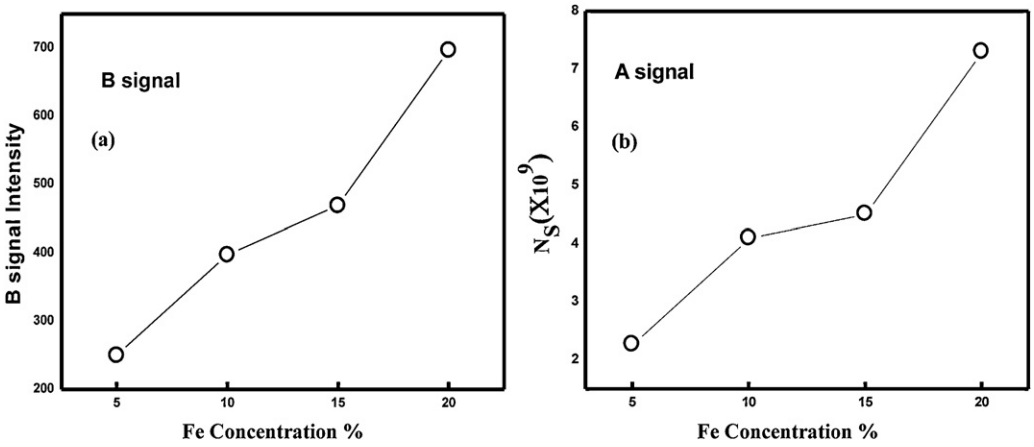

Fig. 12. (a) Fe concentration dependence of $g \sim 4.3$ signal intensity. (b) Number of spins (N_s) participating in the resonance for $g \sim 2.01$ broad signal as a function of Fe concentration.

Table 4
g values of Fe doped CdS nanopowders.

Sample	'g' value	
	Signal A	Signal B
$Cd_{0.95}Fe_{0.05}S$	2.012873	4.31456
$Cd_{0.9}Fe_{0.1}S$	2.012158	4.31504
$Cd_{0.85}Fe_{0.15}S$	2.009751	4.32301
$Cd_{0.8}Fe_{0.2}S$	1.981503	4.36848

randomly substitutes the Cd^{2+} ions. The room-temperature ESR spectrum of Fe doped CdS nanopowders consists of superposition of two overlapping signals, an intense and very broad signal with $g \sim 2.01$ (signal A), and relatively weak and narrow signals at $g \sim 4.3$ (signal B). Table 4 shows *g* values of Fe doped CdS nanopowders. The less intense peak around $g \sim 4.3$ is attributed to isolated Fe^{3+} ions in site of tetrahedral symmetry field [29]. Since Cd has a tetrahedral coordination by S, and since signal B intensity increases (Fig. 12(a)) with Fe doping concentration, it may be arising from Fe^{3+} as substitutional impurity for Cd in CdS. Cd vacancies would have to be postulated in such a situation, to compensate for the additional positive charges brought in by Fe^{3+}.

The number of spins (N_s) participating in the resonance [30] for broad signal has been calculated and is shown in Fig. 12(b). From this figure one can observe that the number of spins participating in the resonance increases with increasing doping percentage. In case of Fe doped ZnS nanoparticles, ESR signal intensity decreases with increasing Fe concentration due to clustering of Fe ions [12] or interaction between two adjacent Fe^{3+} sites through the sulfide bridges leading to suppression of free spins [13]. The intensity of signal A, increasing with increasing Fe^{3+} content, cannot possibly be coming from isolated substitutional or interstitial position in CdS. This intense and broad peak at $g \sim 2.01$ can be assigned to strongly interacting ferric ions, whose origin is yet to be ascertained.

We evaluated the effect due to stirring time and aging with different intervals of time after the preparation. We did not observe any major change in the pure as well as the Fe doped CdS samples with time. Some of the earlier studies indicated that the particle size arise in between 4.3 and 4.6 nm [31] within 0–10 days of preparation. But in our case we have not observed any changes in XRD spectrum even after two months indicating that the particles must be quite stable. Also, the properties like Raman, UV-Visible, Photoluminescence emission and excitation remained the same for two months after the preparation.

4. Conclusions

Phase purity of all samples studied through XRD, FTIR and Raman. Due to the quantum confinement effect, UV–Vis absorption spectrum for pure and Fe doped CdS powders are blue-shifted relative to bulk CdS. Pure and doped CdS nanopowders emission peak maximum at 404 nm. We observed emission from band edge states and localization of these excited states in all samples even at room temperature. The electron spin resonance spectra of Fe doped CdS exhibit two distinct signals at $g \sim 4.3$ and $g \sim 2$ which are characteristic of Fe^{3+} ions.

Acknowledgments

We are thankful to Prof. C.S. Sunandana for his constant help and many fruitful discussions. Authors thank C.H. Suresh, CIL, HCU for the help with the ESR recording. H. Sekhar thanks CAS for financial support. DNR acknowledges DST-ITPAR program for the financial support.

References

[1] J. Hana, C. Liao, T. Jiang, C. Spanheimer, G. Haindl, G. Fu, V. Krishnakumar, K. Zhao, A. Klein, W. Jaegermann, J. Alloys Compd. 509 (2011) 5285.
[2] H. Murai, T. Abe, J. Matsuda, H. Sato, S. Chiba, Y. Kashiwaba, Appl. Surf. Sci. 244 (2005) 351.
[3] N. Kouklin, L. Menon, A.Z. Wong, D.W. Thompson, J.A. Woollam, P.F. Williams, S. Bandyopadhyaya, Appl. Phys. Lett. 79 (2001) 4423.
[4] X. Duan, Y. Huang, R. Agarwal, C.M. Lieber, Nature 421 (2003) 241.
[5] N. Venkatram, D. Narayana Rao, M.A. Akundi, Optics Exp. 13 (2005) 867.
[6] M. Bruchez Jr., M. Moronne, P. Gin, S. Weiss, A. Paul Alivisatos, Science 281 (1998) 2013.
[7] J. He, G.D. Scholes, Y.L. Qu, W. Ji, J. Appl. Phys. 104 (2008) 023110.
[8] J. Franc, J. Hlavka, S. Nespurek, I. Zhivkov, Sol. Energy Mater. Sol. Cells 90 (2006) 2924.
[9] S. Tsoi, I. Miotkowski, S. Rodriguez, A.K. Ramdas, H. Alawadhi, T.M. Pekarek, Phys. Rev. B 72 (2005) 155207.
[10] S.B. Singh, M.V. Limaye, S.K. Date, S. Gokhale, S.K. Kulkarni, Phys. Rev. B 80 (2009) 235421.
[11] X. Lu, I. Miotkowski, A.K. Ramdas, S. Rodriguez, Phys. Rev. B 76 (2007) 035208.
[12] P.H. Borse, N. Deshmukh, R.F. Shinde, S.K. Date, S.K. Kulkarni, J. Mater. Sci. 34 (1999) 6087.
[13] S. Sambasivama, B.K. Reddy, A. Divyaa, N. Madhusudhana Rao, C.K. Jayasankar, B. Sreedhar, Phys. Lett. A 373 (2009) 1465.
[14] M. Thambidurai, N. Muthukumarasamy, S. Agilan, N. Murugan, N. Sabari Arul, S. Vasantha, R. Balasundaraprabhu, Solid State Sci. 12 (2010) 1554.
[15] B. Tripathi, F. Singh, D.K. Avasthi, A.K. Bhati, D. Das, Y.K. Vijay, J. Alloys Compd. 454 (2008) 97.
[16] P.K. Khanna, N. Singh, J. Lumin. 127 (2007) 474.
[17] J. Butty, N. Peyghambarian, Y.H. Kao, J.D. Mackenzie, Appl. Phys. Lett. 69 (1996) 3224.
[18] H. Wang, P. Fang, Z. Chen, S. Wang, J. Alloys Compd. 461 (2008) 418.
[19] J.K. Furdyna, J. Appl. Phys. 64 (1988) 29.
[20] K. Nomura, C.A. Barrero, J. Sakuma, M. Takeda, Phys. Rev. B 75 (2007) 184411.

[21] J. Liu, C. Zhao, Z. Li, J. Chen, H. Zhou, S. Gu, Y. Zeng, Y. Li, Y. Huang, J. Alloys Compd. 509 (2011) 9428.
[22] D. Routkevitch, T.L. Haslett, L. Ryan, T. Bigioni, C. Douketis, S. Moskovits, Chem. Phys. 210 (1996) 343.
[23] D.R. Chuu, C.M. Dai, Phys. Rev. B 45 (1992) 11805.
[24] L. Zeiri, I. Patla, S. Acharya, Y. Golan, S. Efrima, J. Phys. Chem. C 111 (2007) 11843.
[25] Y. Cai Zhang, W. Wei Chen, X. Ya Hu, Cryst. Growth Des. 7 (2007) 580.
[26] L. Spanhel, M. Haase, H. Weller, A. Henglein, J. Am. Chem. Soc. 109 (1987) 5649.
[27] L. Sapanhel, M.A. Anderson, J. Am. Chem. Soc. 112 (1990) 2278.
[28] J. Zhan, X. Yang, D. Wang, S. Li, Y. Xie, Y. Xia, Y. Qian, Adv. Mater. 12 (2000) 1348.
[29] M. Jiang, J. Terra, A.M. Rossi, M.A. Morales, S.E.M. Baggio, D.E. Ellis, Phys. Rev. B 66 (2002) 224107.
[30] C.S. Sunandana, Bull. Mater. Sci. 21 (1998) 1.
[31] B. Saraswathi Amma, K. Ramakrishna, M. Pattabi, J. Mater. Sci.: Mater. Electron. 18 (2007) 1109.